bio-protocol

Open Access

Published: Oct 05, 2025

Artificial Metalloenzymes in Artificial Sanctuaries Through Liquid–Liquid Phase Separation

Kaixin Wang, Guangjie Zhang, Lei Zhang, Yugang Bai* and Tong Wu*

State Key Laboratory of Chemo- and Bio-Sensing, School of Chemistry and Chemical Engineering, Hunan University, Changsha, Hunan, China
*For correspondence: baiyugang@hnu.edu.cn; tongwu@hnu.edu.cn

Abstract

Artificial metalloenzymes (ArMs) hold great promise for expanding the toolbox of non-natural transformations usable in living systems, such as cells, plants, and animals. However, their practical application remains challenging, primarily due to their unsatisfactory stability and inefficient intracellular assembly. We recently reported a new strategy, called artificial metalloenzymes in artificial sanctuaries (ArMAS) through liquid–liquid phase separation (LLPS), to enhance the performance of ArMs in cells by placing them in more friendly artificial microenvironments. Here, this protocol describes the detailed method for using this ArMAS–LLPS strategy, a robust way to create artificial compartments using an ArM protein scaffold through LLPS and construct ArMs within using self-labeling cofactor anchoring reactions. In detail, in *Escherichia coli*, membraneless protein condensates are formed by expressing a self-labeling fusion protein, HaloTag-SNAPTag (HS) and act as intracellular sanctuaries. Simultaneously, the HS scaffolds enable site-specific, bioorthogonal conjugation with synthetic metal cofactors, facilitating efficient ArM formation within the LLPS domains. This strategy can significantly enhance the intracellular catalytic activity and stability of the named HS-based ArMs, allowing whole-cell catalysis to be performed to enable abiotic transformations both in vitro and in vivo. The protocol provides a proof-of-concept approach for researchers aiming to develop stable ArM-based whole-cell catalytic systems for synthetic biology and therapeutic applications.

Key features

- Describes a robust and reproducible protocol for constructing artificial metalloenzymes (ArMs) in living *E. coli* cells using protein-driven liquid–liquid phase separation (LLPS).
- Demonstrates how intracellular LLPS regions can serve as protective catalytic microenvironments, significantly improving ArM stability and catalytic turnover.
- Applicable to various abiotic catalytic transformations, including olefin metathesis.

Keywords: Artificial metalloenzyme, Whole-cell catalyst, Liquid–liquid phase separation, Compartmentalization, Microenvironment

This protocol is used in: Nat Chem Biol (2025), DOI: 10.1038/s41589-024-01819-7

Graphical overview

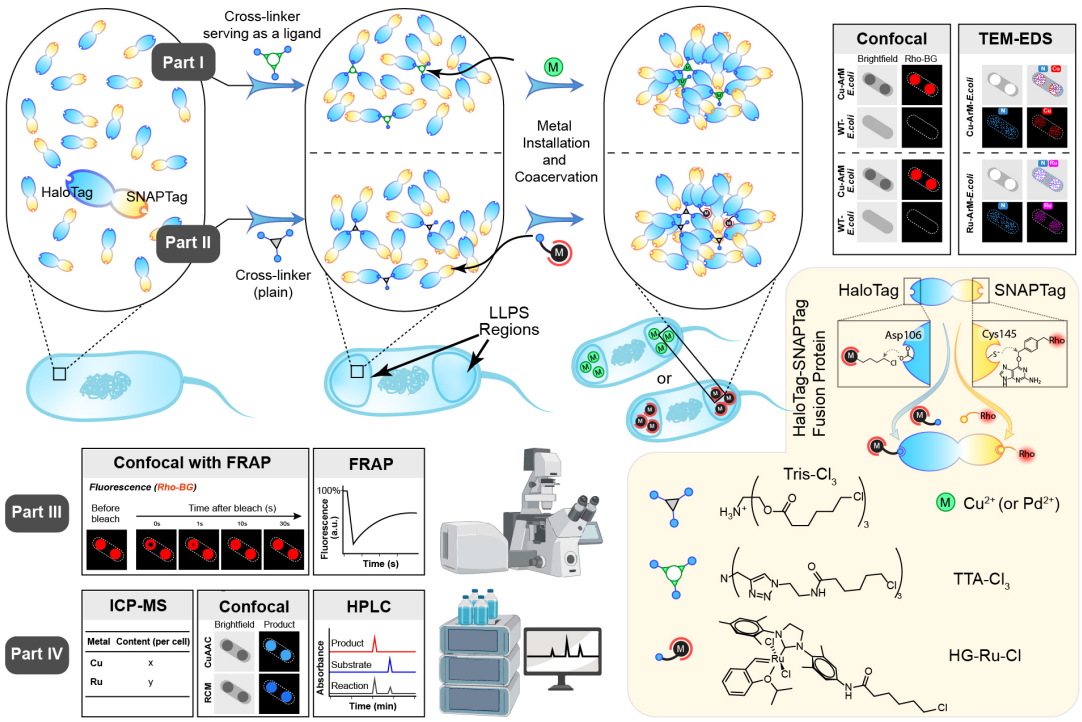

A cartoon illustration of the artificial metalloenzymes in artificial sanctuaries through liquid–liquid phase separation (ArMAS–LLPS) strategy using HaloTag-SNAPTag (HS) fusion protein as the artificial metalloenzyme (ArM) scaffold. In part I, a ligand-crosslinker was used to initiate the LLPS, followed by metal ion cofactor binding on the ligand to form ArMs inside the LLPS regions. In part II, a crosslinker without metal-coordinating function was used to initiate the LLPS, followed by metal complex cofactor anchoring on the HaloTag side of the HS scaffold to form ArMs inside the LLPS regions. In part III, fluorescence recovery after photobleaching (FRAP) analysis is performed to verify the liquid-like properties of the phase-separated protein. In part IV, various assays are conducted to evaluate the catalytic activity enhanced by the ArMAS–LLPS technology.

Background

Since ancient times, whole-cell catalysts have been widely used as natural tools for chemical transformation—from fermentation starters used in brewing to *Penicillium* species employed in penicillin production. These systems have played a critical role in enabling low-cost and large-scale manufacturing of chemicals. In recent years, whole-cell catalysts equipped with artificial metalloenzymes (ArMs) have emerged as a novel hybrid catalytic platform that has attracted growing attention [1,2]. ArMs integrate synthetic metal cofactors with natural protein scaffolds to catalyze abiotic reactions, thereby significantly expanding the scope of enzyme catalysis [4–9]. Incorporating ArMs into whole-cell systems not only enables a broad range of engineered reactions [10,11] but also helps to address challenges such as the high purification cost, limited environmental stability, and poor membrane permeability typically associated with ArMs delivery in cellulo and in vivo [1,12,13].

However, efficient integration of ArMs into whole cells remains challenging due to the complexity of anchoring synthetic metal cofactors onto protein scaffolds within the intracellular environment. Although strategies using high-affinity inhibitors or substrate analogs have been developed to simplify this process, they often fail to offer sufficient protection for sensitive metal cofactors, leading to limited ArM stability in vivo [14–16]. To address this issue, we proposed the artificial metalloenzymes in artificial sanctuaries (ArMAS)–liquid–liquid phase separation (LLPS) strategy, which aims at the construction of artificial intracellular compartments used as dedicated sanctuaries for abiotic catalysis, enhancing the intracellular stability of ArMs [17,18]. These compartments are formed via protein-mediated, minor crosslinking-initiated LLPS, which offers spatial segregation while allowing controlled exchange of materials with the surrounding cytoplasm.

This protocol describes the exact way to establish catalytic "shelters" by inducing controlled LLPS of ArM scaffold proteins, thereby protecting catalytic activity within the cell. HaloTag-SNAPTag (HS), a self-labeling fusion protein, is selected as the model ArM scaffold. The HaloTag side enables bioorthogonal covalent conjugation with alkyl chloride–modified metal cofactors so that ArMs can form, while the SNAPTag provides an orthogonal labeling handle for site-specific conjugation to benzylguanine-functionalized molecules. This dual-tag design not only allows efficient intracellular assembly of ArMs within the condensates formed by HS-LLPS but also offers a strategy to incorporate additional probes or modulators—such as fluorescent labels or crosslinkers—to track, stabilize, or tune the catalytic shelters. This protocol provides a detailed step-by-step procedure for each step in the creation of a whole-cell catalytic system based on ArMAS–LLPS in *Escherichia coli*, including protein expression, LLPS induction, ArM assembly in cellulo, and performance testing.

Materials and reagents

Biological materials

1. Competent cells *E. coli* strain BL21 (DE3) (*Tsingke*, catalog number: DLC201)
2. Plasmid containing HS protein: pET-21d-HS (Figure 1)

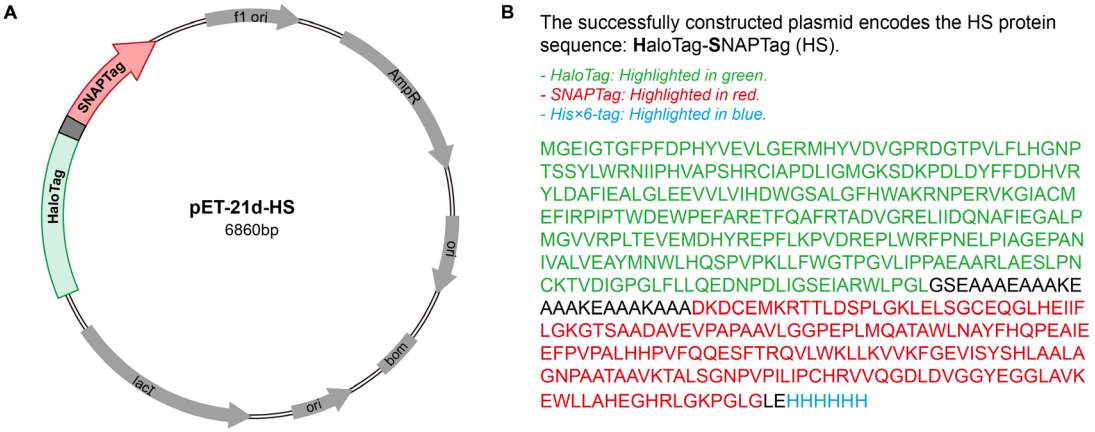

Figure 1. Plasmid map for the HaloTag-SNAPTag (HS) constructs used in the experiment. (A) Plasmid map of the HS expression construct in the pET-21d vector. (B) Amino acid sequence of the HS fusion protein.

Reagents

1. Ampicillin (Macklin, catalog number: A6265)
2. Dimethyl sulfoxide (DMSO) (Macklin, catalog number: D6258)
3. Methanol (MeOH) (Macklin, catalog number: M813907)
4. 4-Ethynylanisole (4-EA) (Macklin, catalog number: M813630)
5. 1,4-Dioxane (Macklin, catalog number: D807836)
6. Magnesium chloride ($MgCl_2$) (Macklin, catalog number: M813763)
7. Sodium chloride (NaCl) (Macklin, catalog number: S805275)
8. Phosphate buffered saline (PBS), 1× (pH 7.4) (Servicebio, catalog number: G4202-500ML)
9. Acetonitrile (ACN) (Macklin, catalog number: A800362)
10. Glutathione (GSH) (Macklin, catalog number: G6268)
11. Copper(II) sulfate hydrate ($CuSO_4 \cdot 5H_2O$) (Macklin, catalog number: 767480)
12. Sodium ascorbate (NaAsc) (Leyan, catalog number: LY-TRCS612200)
13. Isopropyl β-D-1-thiogalactopyranoside (IPTG) (Bomeibio, catalog number: PI5502-25g)
14. LB medium mix powder (Hopebio, catalog number: HB0128)
15. Nitric acid 65% (SCR, catalog number: 10014518)

Solutions

1. LB medium (see Recipes)
2. IPTG 1 M (see Recipes)
3. $CuSO_4·5H_2O$ 1 M (see Recipes)
4. NaAsc 1 M (see Recipes)
5. GSH 2 M (see Recipes)
6. TTA-Cl_3 15.7 mg/mL (see Recipes)
7. Tris-Cl_3 10.4 mg/mL (see Recipes)
8. Rhodamine-labeled benzylguanine (Rho-BG) 15.7 mg/mL (see Recipes)
9. 5-Hydroxy-2-vinylphenol acrylate (HVPA) 20 mM (see Recipes)
10. Diallylpropylene dibenzoate (DAPB) 100 mM (see Recipes)
11. Ethynyldiphenylmethyl allyl ether (EnDA) 200 mM (see Recipes)
12. 3-azido-7-hydroxycoumarin (AzHCou) 25 mM (see Recipes)
13. 4-EA 50 mM (see Recipes)

Note: The structures of TTA-Cl_3, Tris-Cl_3, Rho-BG, HVPA, DAPB, EnDA, and AzHCou are shown in Figure 2.

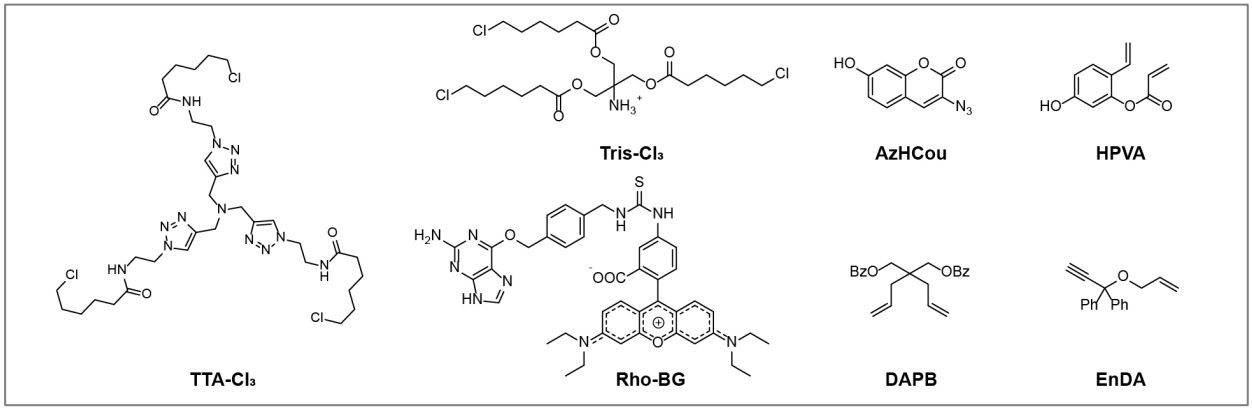

Figure 2. Chemical structures of non-commercial reagents used in this article. TTA-Cl_3, Tris-Cl_3, and Rho-BG were synthesized following [17]; AzHCou was synthesized following [19]; HVPA was synthesized following [20]; and DAPB and EnDA were synthesized following [21].

Recipes

1. LB medium (500 mL)

Reagent	Final concentration	Quantity or volume
LB medium mix powder	25 g/L	12.5 g
ddH_2O	n/a	500 mL
Total	n/a	500 mL

Note: Autoclave at 121 °C for 30 min and aliquot. Store at RT.

2. IPTG 1 M (2 mL)

Reagent	Final concentration	Quantity or volume
IPTG	1 M	476.6 mg
ddH_2O	n/a	2 mL
Total	n/a	2 mL

Note: Sterilize by filtration and store at -20 °C for up to one year.

3. $CuSO_4·5H_2O$ 1 M (1 mL)

Reagent	Final concentration	Quantity or volume
$CuSO_4·5H_2O$	1 M	249.7 mg
ddH_2O	n/a	1 mL
Total	n/a	1 mL

4. NaAsc 1 M (1 mL)

Reagent	Final concentration	Quantity or volume
NaAsc	1 M	198.1 mg
ddH_2O	n/a	1 mL
Total	n/a	1 mL

Note: Prepare the solution fresh each day and sterilize it by filtration before use.

5. GSH 2 M (2 mL)

Reagent	Final concentration	Quantity or volume
GSH	2 M	1.229 g
ddH_2O	n/a	2 mL
Total	n/a	2 mL

Note: Sterilize by filtration and store at -20 °C for up to one year.

6. TTA-Cl_3 15.7 mg/mL (1 mL)

Reagent	Final concentration	Quantity or volume
TTA-Cl_3	20 mM	15.7 mg
DMSO	n/a	1 mL
Total	n/a	1 mL

Note: Sterilize by filtration.

7. Tris-Cl_3 10.4 mg/mL (1 mL)

Reagent	Final concentration	Quantity or volume
Tris-Cl_3	20 mM	10.4 mg
DMSO	n/a	1 mL
Total	n/a	1 mL

Note: Sterilize by filtration.

8. Rho-BG 15.7 mg/mL (1 mL)

Reagent	Final concentration	Quantity or volume
Rho-BG	15.7 mg/mL (20 mM)	15.7 mg
DMSO	n/a	1 mL
Total	n/a	1 mL

Note: Sterilize by filtration.

9. HVPA 20 mM (1 mL)

Reagent	Final concentration	Quantity or volume
HVPA	20 mM	3.80 mg
DMSO	n/a	1 mL
Total	n/a	1 mL

Note: Sterilize by filtration.

10. DAPB 100 mM (1 mL)

Reagent	Final concentration	Quantity or volume
HVPA	100 mM	36.44 mg
DMSO	n/a	1 mL
Total	n/a	1 mL

Note: Sterilize by filtration.

11. EnDA 200 mM (1 mL)

Reagent	Final concentration	Quantity or volume
HVPA	200 mM	49.67 mg
DMSO	n/a	1 mL
Total	n/a	1 mL

Note: Sterilize by filtration.

12. AzHCou 50 mM (0.5 mL)

Reagent	Final concentration	Quantity or volume
HVPA	50 mM	5.08 mg
DMSO	n/a	0.5 mL
Total	n/a	0.5 mL

Note: Sterilize by filtration.

13. 4-EA 50 mM (0.5 mL)

Reagent	Final concentration	Quantity or volume
HVPA	50 mM	3.30 mg
DMSO	n/a	0.5 mL
Total	n/a	0.5 mL

Note: Sterilize by filtration.

Laboratory supplies

1. Automatic pipettes (ThermoFisher Scientific)
2. Pipette tips (Servicebio)
3. 2 mL microcentrifuge tube (Servicebio, catalog number: EP-200-M）
4. 15 mL centrifuge tube (Servicebio, catalog number: EP-1500-BJ）
5. 12 mL bacteria culture tube (Bikeman Bio, catalog number: 110408020)
6. Syringe filter (0.22 μm) (Merck Millipore, catalog number: C134954)

Equipment

1. Floor incubator shaker with cooling (Zhichu, model: ZQLY-180)
2. Biochemical incubator (Lichen, model: SPX-250B)
3. Ice machine (Meiling, model: MZB-25ZS)
4. Clean bench (Lichen, model: SW-CJ-1FD)
5. Biological safety cabinet (Esco, model: AC2-4S1)
6. Microplate reader (Thermo Fisher Scientific, model: Multiskan FC)
7. pH meter (Oustor, model: PHS-3C)
8. Fully automatic autoclave sterilizer (STIK, model: MJ-78A)
9. Vortex mixer (Scientific Industries, model: Vortex-Genie 2)
10. Centrifuge (Eppendorf, model: 5424R/5810R)
11. Microvolume spectrophotometer (Thermo Fisher Scientific, model: NanoDrop-2000)
12. Ultrapure water system (Merck Millipore, model: Elix 3)
13. Ultrasonic cell crusher (Scientz, model: JY92-IIN)
14. Confocal microscope (Nikon, model: A1RMP)
15. Confocal microscope with FRAP module (Carl Zeiss Microscopy, model: LSM980)
15. Inductively coupled plasma-mass spectrometer (ICP-MS) (Agilent Technologies, model: 7900)
16. High-performance liquid chromatography (HPLC) (Waters, model: 600; and Agilent Technologies, model: 1260)

17. Transmission electron microscope (TEM) equipped with an adapter for energy-dispersive X-ray spectroscopy (EDS) (JEOL, model: JEM-2100 Plus)

Procedure

Part I: Construction of Cu-ArM in artificial compartments created in engineered *E. coli*

A. Assembly of HS fusion protein-based artificial compartments

1. Inoculate *E. coli* BL21 (DE3) cells carrying plasmids encoding the HS protein into 5 mL of LB medium containing 100 μg/mL ampicillin.
2. Incubate the culture at 37 °C with shaking at 220 rpm until the optical density at 600 nm (OD_{600}) reaches approximately 0.6, which typically requires approximately 3 h.
3. Add **IPTG** (5 μL, 1 M, final concentration 1 mM) to induce HS expression, immediately followed by the addition of **TTA-Cl_3** (9 μL, 15.7 mg/mL dissolved in DMSO) to reach a final concentration of 36 μM.
4. Further incubate the culture at 18 °C with shaking at 220 rpm for 18 h to allow compartment formation.
5. Harvest cells by centrifugation at 9,000× *g* for 2 min at 4 °C and discard the supernatant.
6. Resuspend the pellet in 1 mL of PBS and then centrifuge and wash three times under the same conditions to remove excess reagents.
7. After the final wash, resuspend the pellet in an appropriate volume of PBS to adjust the OD_{600} to 0.6, generating a suspension of bacteria containing artificial compartments.
8. Place a drop of this suspension on a glass slide for observation using a confocal microscope. Confocal images of the compartmentalized bacteria are shown in Figure 3A.

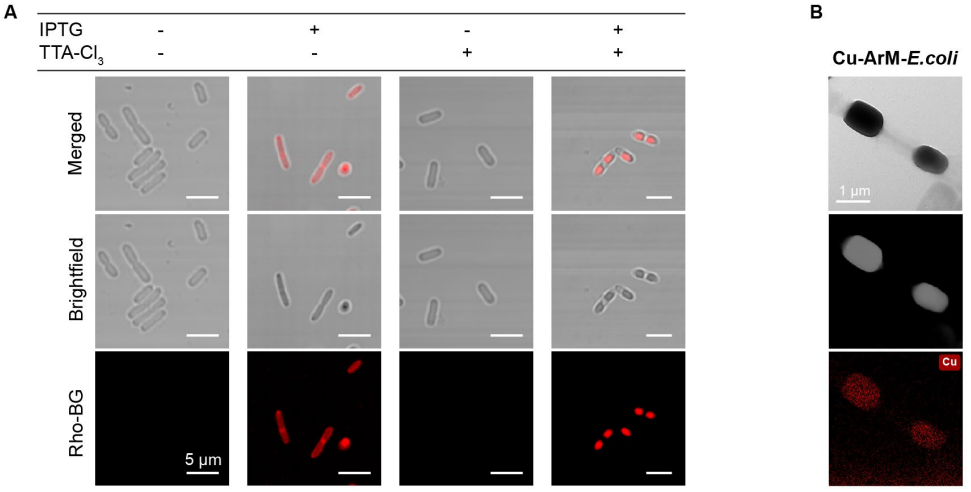

Figure 3. TTA-Cl_3-induced formation of artificial compartments and the incorporation of Cu-ArMs within them. (A) Confocal microscopic images of HaloTag-SNAPTag (HS)-expressing *E. coli* under different treatment conditions: IPTG only, IPTG+TTA-Cl_3, and TTA-Cl_3 only. The HS fusion protein was fluorescently labeled using Rho-BG. The images clearly demonstrate that the presence of the crosslinker (TTA-Cl_3) is essential for inducing HS protein condensation in bacterial cells. (B) Transmission electron microscope–energy-dispersive X-ray spectroscopy (TEM–EDS) image of HS-expressing *E. coli* containing Cu-HS-ArM, showing apparent enrichment of copper within the LLPS-based artificial compartments. ArM: artificial metalloenzyme.

B. Cu-ArM assembly within artificial compartments

1. Mix a 1 mL aliquot of the compartmentalized *E. coli* suspension prepared above with $CuSO_4$ solution (10 μL, 1 mM).
2. Incubate the mixture at 37 °C for 30 min to enable the TTA moieties within the compartments to chelate copper ions.
3. Collect the cells by centrifugation at 9,000× *g* for 2 min at 4 °C and remove the supernatant.

4. Resuspend the pellet in 1 mL of PBS and wash three times by repeating centrifugation and resuspension under the same conditions to eliminate free copper ions.
5. After the final wash, resuspend the pellet in PBS to an OD_{600} of 0.6, yielding a working suspension of *E. coli* harboring Cu-ArM within the artificial compartments.
6. Representative confocal and TEM images of the *E. coli* cells containing Cu-ArM assembled within the artificial compartments are shown in Figure 3B.

Part II: Formation of Ru-ArM in artificial compartments of *E. coli*

A. Formation of artificial compartments based on HS fusion protein

To generate artificial compartments using the HS scaffold, follow the procedure described in Part I.A, with the only modification being the replacement of **TTA-Cl$_3$** (9 µL, 15.7 mg/mL in DMSO, final concentration 36 µM) with **Tris-Cl$_3$** (9 µL, 10.4 mg/mL in DMSO, final concentration 36 µM). Then, characterize the resulting *E. coli* cells by confocal microscopy to visualize compartment formation, as shown in Figure 4A.

B. Assembly of Ru-ArM within the artificial compartments

1. Prepare a 1 mL suspension of *E. coli* cells containing artificial compartments (Figure 4A). Add **HG-Ru-Cl** solution (5 µL, 20 mM in dioxane, final concentration 100 µM) to initiate metal cofactor conjugation.
2. Incubate the mixture at 18 °C for 8 h to allow conjugation between the protein scaffold and the ruthenium complex.
3. Pellet cells by centrifugation at 9,000× *g* for 2 min at 4 °C and discard the supernatant.
4. Resuspend the pellet in 1 mL of PBS and wash three times by repeating the centrifugation step (9,000× *g* for 2 min at 4 °C) to remove unbound metal complexes.
5. After the final wash, resuspend the pellet in PBS containing 0.1 M $MgCl_2$ (pH 7.4) and adjust to an OD_{600} of 0.6 to obtain the working suspension of *E. coli* cells harboring Ru-ArM within the LLPS-based compartments.
6. Characterize *E. coli* cells with Ru-ArM-containing artificial compartments by confocal microscopy and TEM, as shown in Figure 4B.

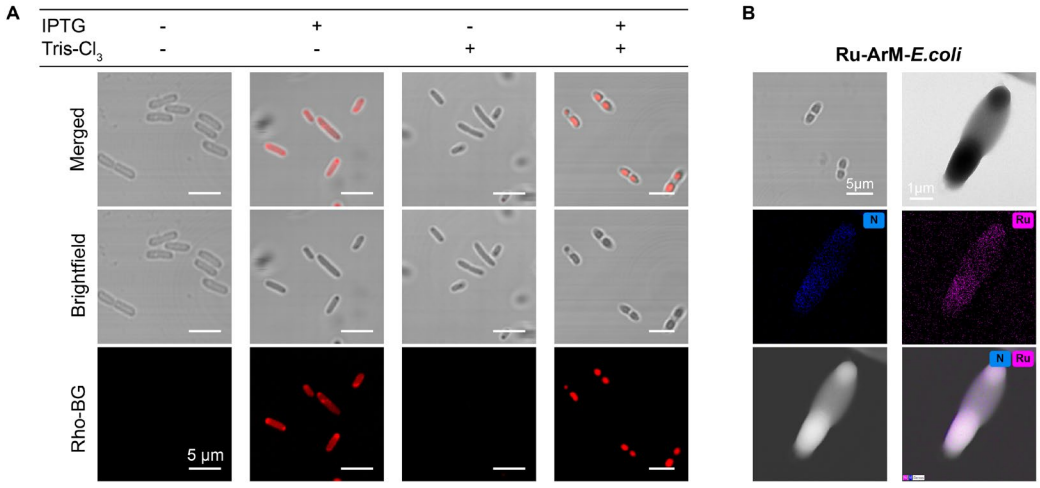

Figure 4. Tris-Cl$_3$-induced formation of artificial compartments and the incorporation of Ru-ArMs within them. (A) Confocal microscopy images of HaloTag-SNAPTag (HS)-expressing *E. coli* under different treatment conditions: **IPTG** only, **IPTG**+**Tris-Cl$_3$**, and **Tris-Cl$_3$** only. The HS fusion protein was fluorescently labeled with Rho-BG. The results indicate that the presence of the crosslinker is essential for inducing HS protein condensation within bacterial cells. (B) Transmission electron microscope–energy-dispersive X-ray spectroscopy (TEM–EDS) image of *E. coli* expressing Ru-HS-ArM, showing clear enrichment of ruthenium within the LLPS-based artificial compartments. ArM: artificial metalloenzyme. LLPS: Liquid–liquid phase separation.

Part III: Characterization of the liquid-like properties of phase-separated HS protein using the intracellular fluorescence recovery after photobleaching (FRAP) technique

1. Add **Rho-BG** dye to the previously prepared suspension of *E. coli* cells containing artificial compartments (OD_{600} = 0.6) to a final concentration of 50 μM. Incubate the cells at 37 °C for 30 min to allow for fluorescent labeling.
2. Centrifuge the cell suspension at 9,000× *g* for 2 min at 4 °C and remove the supernatant. Resuspend the pellet in 1 mL of PBS.
3. Repeat the washing step three times under the same conditions (9,000× *g* for 2 min at 4 °C) to remove any unbound **Rho-BG** dye that remained outside the cells.
4. After the final wash, resuspend the pellet in PBS and adjust to an OD_{600} of 0.6 to prepare the final cell suspension.
5. Place a droplet of stained suspension on a microscope slide for confocal microscope imaging and FRAP analysis.
6. Perform confocal FRAP experiments using a Carl Zeiss LSM980 confocal microscope equipped with a 63× oil immersion objective. For intracellular FRAP, select a circular region of interest (ROI) with a diameter of approximately 0.3 μm within one half of an LLPS protein condensate (about 0.5 μm from the condensate edge). In our work, the **Rho-BG**-labeled HS protein was excited using a 561 nm laser. Image acquisition for the pre-bleach and post-bleach phases was conducted at a low laser intensity of 1.8%. The imaging sequence was initiated by capturing two pre-bleach images. Then, the ROI was bleached with high-intensity (100%) laser pulses until the fluorescence signal decreased to 20% of its initial intensity. Following bleaching, fluorescence recovery was monitored by acquiring a series of 112 post-bleach images. In total, 114 images were captured with a time interval of 0.78 s between frames. The microscope's time-lapse acquisition software (time measurement) was used to track fluorescence recovery within the ROI. A detailed description of the fluorescence recovery analysis can be found in Data analysis A.

Part IV: Intracellular abiotic catalysis mediated by ArMs in compartmentalized *E. coli*

A. Cu-ArM-catalyzed CuAAC reaction

1. Mix a 500 μL aliquot of the *E. coli* suspension containing Cu-ArM (Cu-ArM-HS-*E. coli*) prepared as described in Part I.B with **4-EA** (10 μL, 50 mM in DMSO) and **AzHCou** (10 μL, 50 mM in DMSO). Add **NaAsc** (1 μL, 1 M) and vortex the mixture for 5 s to initiate the reaction.
2. After incubation at 37 °C for 24 h, add **GSH** (1 μL, 2 M) and 1.5 mL methanol.
3. Lyse the treated cells by sonication on ice for 20 min (40% power, 1-s pulses with 2-s intervals).
4. Vortex the lysate for 30 min.
5. Centrifuge the mixture at 9,000× *g* for 2 min at 4 °C to separate cell debris from the soluble fluorescent product.
6. Collect the supernatant and analyze the products qualitatively and quantitatively using HPLC or fluorescence measurements to determine product concentration.
7. Separately, take another 500 μL of Cu-ArM-containing *E. coli* suspension and centrifuge. Discard the supernatant, add 100 μL of concentrated nitric acid to the pellet, and digest at room temperature for 4 h. Dilute with ultrapure water and determine the actual Cu content in cells by ICP-MS, which serves to calculate the catalyst concentration.
8. The turnover number (TON) is calculated by dividing the product concentration (determined by HPLC or fluorescence) by the catalyst concentration (determined by ICP-MS) and multiplying by any dilution factors used in subsequent sample processing.
9. If quantification was done using fluorometry, fluorescence should be performed with excitation at 410 nm and emission at 480 nm, using fluorescence intensity comparison with authentic standards to determine conversion rates. The fluorescence of the authentic standards must only be measured when they are dissolved in the same medium as the catalysis samples due to the high impact of the environment on these compounds' fluorescence intensity (see Data analysis B for details).

B. Ru-ArM-catalyzed RCM reaction

B1. RCM reaction with HVPA as substrate

1. Aliquot the *E. coli* suspension containing Ru-ArM (Ru-ArM-HS-*E. coli*) prepared in Part II.B into 100 μL portions in pre-cooled 200 μL amber vials. Add **HVPA** (10 μL, 20 mM in DMSO) and then incubate the reaction at 37 °C for 24 h.
2. Withdraw a 50 μL aliquot and quench it with 100 μL of methanol at 0 °C.
3. Lyse the cells by sonication on ice for 20 min (40% power, 1-s pulses with 2-s intervals).
4. Vortex the lysate for 30 min.

5. Centrifuge the mixture at 9,000× *g* for 2 min at 4 °C to separate cell debris and soluble products.
6. Collect the supernatant and quantify the product concentration using HPLC.
7. Separately, take 500 µL of Ru-ArM-containing *E. coli* suspension and centrifuge. Discard the supernatant, add 100 µL of concentrated nitric acid to the pellet, and digest at room temperature for 4 h. Dilute with ultrapure water and determine the actual Ru content in cells by ICP-MS, which serves to calculate the catalyst concentration.
8. The turnover number (TON) [22] is calculated by dividing the product concentration (determined by HPLC) by the catalyst concentration (determined by ICP-MS) and multiplying by any dilution factors used during sample processing (see Data analysis C).
Note: HPLC conditions: flow rate 1 mL/min; column: Agilent ZORBAX SB-C8; mobile phase: H_2O (0.1% TFA): ACN (0.1% TFA) = 45:55.

B2. RCM reaction with DAPB as substrate
1. **HVPA** (10 µL, 20 mM in DMSO) used in Part IV.B1 was replaced by **DAPB** (10 µL, 100 mM in DMSO), with all other steps remaining identical (see Data analysis C).
Note: HPLC conditions: flow rate 1 mL/min; column: Agilent ZORBAX SB-C8; mobile phase: H_2O (0.1% TFA): ACN (0.1% TFA) = 25:75.

B3. RCM reaction with EnDA as substrate
1. HVPA (10 µL, 20 mM in DMSO) used in part IV.B1 was replaced by **EnDA** (10 µL, 200 mM in DMSO), with all other steps remaining identical (see Data analysis C).
Note: HPLC conditions: flow rate 1 mL/min; column: Agilent ZORBAX SB-C8; mobile phase: H_2O (0.1% TFA): ACN (0.1% TFA) = 25:75.

Data analysis

A. Analysis of intracellular FRAP results

Protein aggregates primarily form in two ways: LLPS and liquid–solid phase separation. To verify the liquid-like nature of phase-separated HS protein, FRAP experiments were conducted to monitor molecular diffusion within the aggregates. In LLPS droplets, proteins and other molecules can diffuse freely, allowing the bleached fluorescence area to be rapidly replenished by surrounding molecules, resulting in significant fluorescence recovery. Conversely, in liquid–solid phase separation, molecular mobility is restricted, leading to minimal fluorescence recovery. As shown in Figure 5, clear FRAP recovery was observed within the artificial compartments inside the bacteria, with approximately 60% of the initial fluorescence intensity restored within 12 s post-bleaching. This indicates that the HS protein condensates exhibit liquid-like properties. Such liquid characteristics are essential for creating effective catalytic compartments: a viable microenvironment must permit material exchange to enable substrates and products to freely enter and exit. These findings not only deepen the understanding of intracellular LLPS compartment properties but also provide an experimental foundation for harnessing these compartments for efficient catalysis.

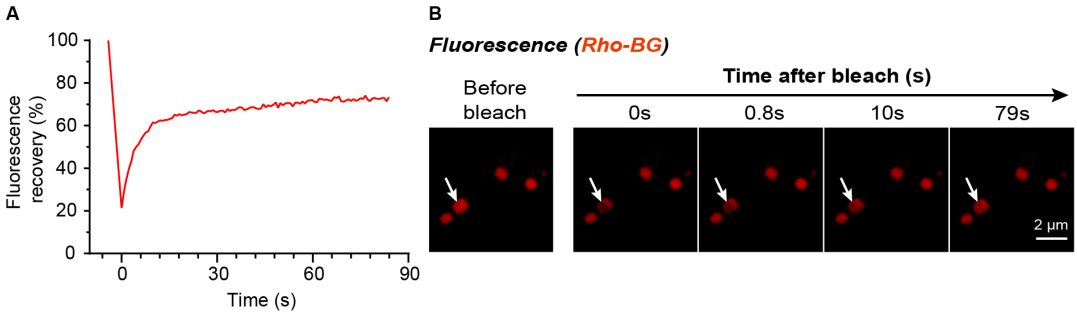

Figure 5. FRAP analysis of the liquid-like phase separation behavior of HaloTag-SNAPTag (HS) protein inside *E. coli*. (A) Fluorescence recovery curve of the bleached region, demonstrating rapid fluorescence restoration indicative of significant molecular diffusion. (B) Representative confocal microscopy images show **Rho-BG**-labeled HS protein

fluorescence before bleaching and at 0, 0.8, 10, and 79 s after bleaching. White arrows indicate the bleached region. Scale bar: 2 μm.

B. Analysis of CuAAC reaction catalyzed by Cu-ArM assembled within artificial compartments

In this study, we employed the widely used copper-catalyzed azide-alkyne cycloaddition (CuAAC) reaction between **AzHCou** and **4-EA** (Figure 6A) as a model to directly observe the intracellular catalysis by Cu-ArM assembled within artificial compartments via confocal microscopy. The results demonstrated that **IPTG** effectively induces the expression of the HS protein, while **TTA-Cl$_3$** triggers LLPS of HS protein inside the cells, leading to the formation of stable artificial compartments. Within these compartments, HS protein acts as a ligand coordinating Cu^{2+} ions, and in the presence of **NaAsc**, Cu(II) is reduced to the catalytically active Cu(I) species. It should be noted that Cu^{2+} and NaAsc were introduced as a pair to give Cu(I); therefore, there are three variables: IPTG, TTA-Cl_3, and Cu^{2+}-plus-NaAsc. The CuAAC reaction proceeds efficiently only when all three conditions—HS protein expression, LLPS formation, and the presence of Cu(I)—are simultaneously met, with catalytic activity predominantly confined to the Cu-ArM-loaded artificial compartments (Figure 6B). Quantitative analysis of fluorescence intensity and TON (Figure 6C, D) further confirms the high catalytic efficiency of this system.

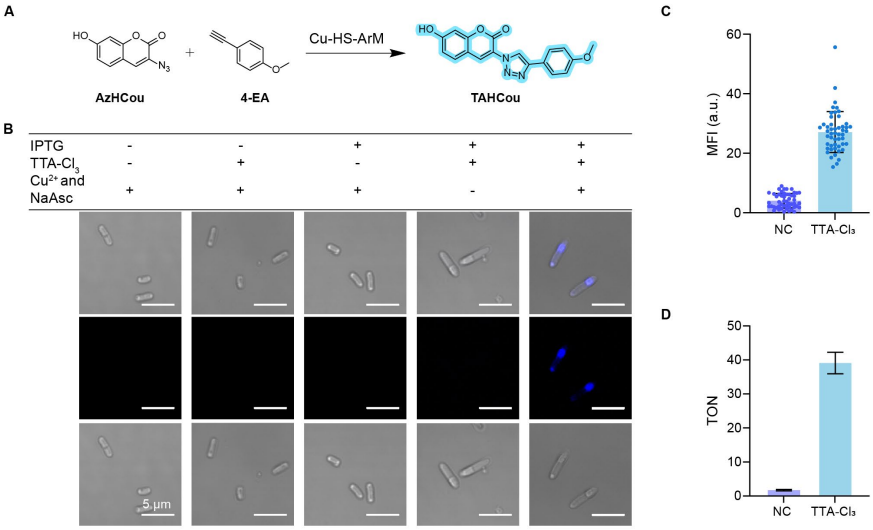

Figure 6. Cu-ArM-loaded artificial compartments catalyze CuAAC reaction in *E. coli*. (A) Schematic representation of the CuAAC reaction between **AzHCou** and **4-EA** catalyzed by Cu-HS-ArM, yielding the fluorescent product **TAHCou**. (B) Confocal fluorescence images of HaloTag-SNAPTag (HS)–*E. coli* under different conditions (±**IPTG**, ±**TTA-Cl$_3$**, ±**Cu^{2+}/NaAsc**). Fluorescent signal from TAHCou was observed only when all four components were present. Scale bars: 5 μm. (C) Quantification of mean fluorescence intensity (MFI), showing significantly higher signal in the **TTA-Cl$_3$**-treated group compared to the negative control (NC, containing **IPTG**, **Cu^{2+}**, and **NaAsc**, but without **TTA-Cl$_3$**). Data displayed as mean ± SD (n = 50). (D) Turnover number (TON) analysis under different conditions, indicating efficient CuAAC catalysis by Cu-ArM assembled within LLPS-based artificial compartments. ArM: artificial metalloenzyme. LLPS: Liquid–liquid phase separation. Data are displayed as mean ± SD, n = 3 independent replicates.

C. Analysis of RCM reaction catalyzed by Ru-ArM assembled within artificial compartments

In this study, we employed **HVPA** as a model substrate for the ruthenium-catalyzed ring-closing metathesis (RCM) reaction, utilizing its intrinsic olefin groups (Figure 7A, C). The catalytic process was directly visualized via confocal fluorescence microscopy. The results demonstrated that IPTG induced the expression of HS protein, while **Tris-Cl$_3$** triggered the formation of LLPS of the expressed protein within *E. coli*, thereby forming intracellular artificial compartments. Simultaneously, the ruthenium cofactor (**HG-Ru-Cl**) was effectively incorporated into the ArM scaffold, generating catalytically active Ru-ArM. The RCM reaction proceeded efficiently only when all three conditions—HS protein expression, LLPS compartmentalization, and Ru cofactor installation—were simultaneously met, indicating that catalysis was mediated by the Ru-ArMs and was confined to the engineered compartments (Figure 7B). Furthermore, three different substrates (**HVPA**, **DAPB**, and **EnDA**) were tested, and product formation was quantified by HPLC (Figure 7F–H), along

with TON calculations to evaluate catalytic performance (Figure 7D, E). These results confirm the feasibility and efficiency of performing Ru-catalyzed abiotic transformations within LLPS-based artificial compartments in living cells.

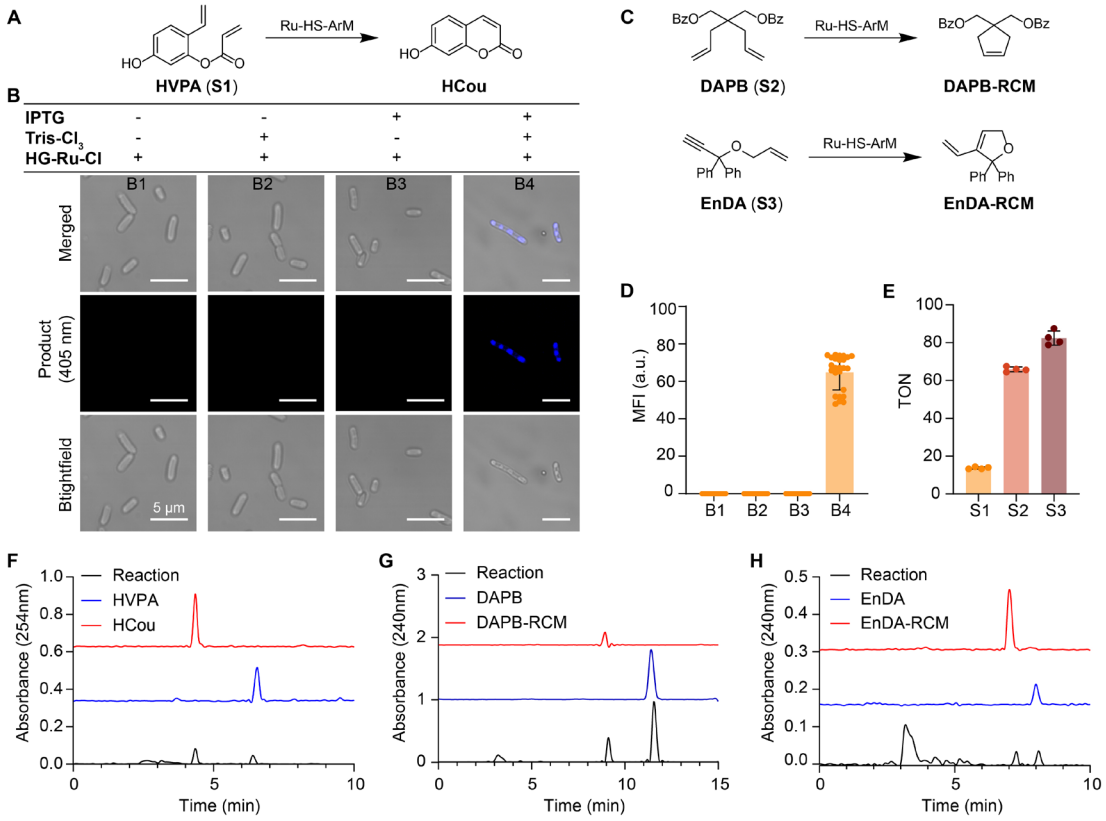

Figure 7. Construction of an intracellular artificial Ru metalloenzyme catalyzing ring-closing metathesis (RCM). (A) Schematic of the conversion of substrate **HVPA** (**S1**) to product **HCou** catalyzed by Ru-HS-ArM. HS: HaloTag-SNAPTag. (B) Fluorescence microscopy images showing intracellular product formation under different conditions (merged: overlay; product: fluorescence at 405 nm; brightfield: brightfield image). B1–B4 correspond to conditions without inducer, without **Tris-Cl**$_3$, without **HG-Ru-Cl**, and with all components, respectively. Scale bar: 5 μm. (C) Schematics of the RCM reaction converting substrates **DAPB** (**S2**) and **EnDA** (**S3**) to **DAPB-RCM** and **EnDA-RCM**, respectively, catalyzed by Ru-HS-ArM. (D) Quantification of mean fluorescence intensity (MFI) under conditions B1–B4; error bars represent standard deviation. Data displayed as mean ± SD (n = 25). (E) Comparison of turnover numbers (TON) for substrates **S1**, **S2**, and **S3**. Data displayed as mean ± SD, n = 4 independent replicates. (F–H) HPLC analysis of substrates and their RCM products: **EnDA** and **EnDA-RCM** (F); **HVPA** and **HCou** (G); and **DAPB** and **DAPB-RCM** (H), with absorbance wavelengths indicated. ArM: artificial metalloenzyme.

Validation of protocol

This protocol or parts of it has been used and validated in the following research article:

- Wu et al [17]. Artificial metalloenzyme assembly in cellular compartments for enhanced catalysis. (Figures 4–8).

General notes and troubleshooting

General notes

1. Our previous study revealed that the linker region connecting the two protein domains serves as the key determinant for HS protein-mediated LLPS in bacteria. This intrinsically disordered region (IDR) provides the structural basis for LLPS

formation. However, experimental validation demonstrated that this structural feature alone is insufficient to drive LLPS unless the protein concentration is very high. The addition of covalent crosslinking compounds (e.g., TTA-Cl_3 or Tris-Cl_3) during protein expression remains essential to effectively induce phase separation and form distinct biomolecular condensates in a more practical manner.
2. To achieve efficient LLPS and clearly visualize the artificial compartments, the bacterial culture density should be kept consistent ($OD_{600} \approx 0.6$) prior to induction to ensure experimental reproducibility.
3. In FRAP experiments, we evaluated the performance of two confocal microscope systems (A1RMP and LSM980). Technical assessment revealed that due to hardware limitations, the A1RMP system could not achieve precise photobleaching of minute regions of interest (ROIs) within bacterial cells, but instead unavoidably bleached an extended area surrounding the target ROI. Based on a comprehensive performance comparison, we strongly recommend employing the LSM980 system or an equivalent state-of-the-art instrument for such high-precision FRAP studies.
4. Some of the substrates used in this protocol exhibit significant chemical instability and are prone to degradation or self-aggregation. To maintain their chemical integrity, we recommend the following preservation protocol: dissolve the substrates in strictly anhydrous DMSO or dioxane to prepare 10–100 mM stock solutions and store at -20 °C protected from light (avoid freeze-thaw cycles). This storage method ensures long-term stability of the substrates.
5. Experimental observations revealed that after induction treatment, *E. coli* cytoplasm typically exhibits random formation of 1–2, or even 3–5, discrete spherical compartments. This randomness in number and distribution is a normal feature of the LLPS process, reflecting the intrinsic property of biomolecular condensates to spontaneously assemble within the confined intracellular environment.

Troubleshooting

Problem 1: LLPS compartment formation is not uniform across all cells.
Possible cause: Repeated freeze-thaw cycles have caused partial plasmid loss within bacteria, resulting in inconsistent protein expression levels.
Solution: Re-transform bacteria and select single clones exhibiting high protein expression levels (>50 mg/L) for subsequent experiments.

Problem 2: Catalytic activity is lower than expected.
Possible causes: (a) Partial substrate degradation due to reasons including but not limited to prolonged storage, repeated freeze-thaw cycles, high temperature storage, or contamination; (b) insufficient intracellular metal loading; (c) suboptimal or incompatible reaction conditions.
Solutions: (a) Prepare fresh stock solutions; (b) within reasonable limits, increase the incubation temperature, concentration, and incubation duration of the metal ligand solution, but avoid shaking incubation; (c) for catalytic reactions, particularly ring-closing metathesis (RCM), the catalytic activity of ArMs at 37 °C is significantly higher than that at 25 °C. Additionally, adding 0.1 M $MgCl_2$ to the PBS buffer is helpful for achieving high RCM reaction activity.

Acknowledgments

Funding support from the National Natural Science Foundation of China (grant no. 22361142830) and the Department of Science and Technology of Hunan Province (grant no. 2024JJ2010 and 2022RC1107) is gratefully acknowledged. The authors thank the Analysis and Testing Center of Hunan University for assistance in characterization.
Specific contributions of each author are as follows: Conceptualization: K.W., Y.B., and T.W.; Investigation: K.W., G.Z., and L.Z.; Writing-Original Draft: K.W. and T.W.; Writing-Review & Editing: T.W. and Y.B.; Funding Acquisition: Y.B. and T.W.; Supervision: Y.B. and W.T.
This protocol has been utilized and validated in a previous study by Wu et al. [17,18], which demonstrated that compartments formed by HS protein-based artificial metalloenzyme assembly in *E. coli* can effectively enhance the catalytic activity of ArMs.

Competing interests

The authors declare no conflicts of interest.

Ethical considerations

There are no ethical considerations associated with this protocol.

Received: June 22, 2025; Accepted: September 02, 2025; Available online: September 16, 2025; Published: October 05, 2025

References

1. Wittwer, M., Markel, U., Schiffels, J., Okuda, J., Sauer, D. F. and Schwaneberg, U. (2021). Engineering and emerging applications of artificial metalloenzymes with whole cells. *Nat Catal.* 4(10): 814–827. https://doi.org/10.1038/s41929-021-00673-3
2. Chordia, S., Narasimhan, S., Lucini Paioni, A., Baldus, M. and Roelfes, G. (2021). In Vivo Assembly of Artificial Metalloenzymes and Application in Whole-Cell Biocatalysis. *Angew Chem Int Ed.* 60(11): 5913–5920. https://doi.org/10.1002/anie.202014771
3. Jeschek, M., Reuter, R., Heinisch, T., Trindler, C., Klehr, J., Panke, S. and Ward, T. R. (2016). Directed evolution of artificial metalloenzymes for in vivo metathesis. *Nature.* 537(7622): 661–665. https://doi.org/10.1038/nature19114
4. Bloomer, B. J., Clark, D. S. and Hartwig, J. F. (2022). Progress, Challenges, and Opportunities with Artificial Metalloenzymes in Biosynthesis. *Biochemistry.* 62(2): 221–228. https://doi.org/10.1021/acs.biochem.1c00829
5. Coelho, P. S., Brustad, E. M., Kannan, A. and Arnold, F. H. (2013). Olefin Cyclopropanation via Carbene Transfer Catalyzed by Engineered Cytochrome P450 Enzymes. *Science (1979).* 339(6117): 307–310. https://doi.org/10.1126/science.1231434
6. Vornholt, T., Christoffel, F., Pellizzoni, M. M., Panke, S., Ward, T. R. and Jeschek, M. (2021). Systematic engineering of artificial metalloenzymes for new-to-nature reactions. *Sci Adv.* 7(4): eabe4208. https://doi.org/10.1126/sciadv.abe4208
7. Key, H. M., Dydio, P., Clark, D. S. and Hartwig, J. F. (2016). Abiological catalysis by artificial haem proteins containing noble metals in place of iron. *Nature.* 534(7608): 534–537. https://doi.org/10.1038/nature17968
8. Renata, H., Wang, Z. J. and Arnold, F. H. (2015). Expanding the Enzyme Universe: Accessing Non-Natural Reactions by Mechanism-Guided Directed Evolution. *Angew Chem Int Ed.* 54(11): 3351–3367. https://doi.org/10.1002/anie.201409470
9. Huang, J., Liu, Z., Bloomer, B. J., Clark, D. S., Mukhopadhyay, A., Keasling, J. D. and Hartwig, J. F. (2021). Unnatural biosynthesis by an engineered microorganism with heterologously expressed natural enzymes and an artificial metalloenzyme. *Nat Chem.* 13(12): 1186–1191. https://doi.org/10.1038/s41557-021-00801-3
10. Davis, H. J. and Ward, T. R. (2019). Artificial Metalloenzymes: Challenges and Opportunities. *ACS Cent Sci.* 5(7): 1120–1136. https://doi.org/10.1021/acscentsci.9b00397
11. Wu, S., Zhou, Y., Gerngross, D., Jeschek, M. and Ward, T. R. (2019). Chemo-enzymatic cascades to produce cycloalkenes from bio-based resources. *Nat Commun.* 10(1): 5060. https://doi.org/10.1038/s41467-019-13071-y
12. Okamoto, Y., Kojima, R., Schwizer, F., Bartolami, E., Heinisch, T., Matile, S., Fussenegger, M. and Ward, T. R. (2018). A cell-penetrating artificial metalloenzyme regulates a gene switch in a designer mammalian cell. *Nat Commun.* 9(1): 1943. https://doi.org/10.1038/s41467-018-04440-0
13. Eda, S., Nasibullin, I., Vong, K., Kudo, N., Yoshida, M., Kurbangalieva, A. and Tanaka, K. (2019). Biocompatibility and therapeutic potential of glycosylated albumin artificial metalloenzymes. *Nat Catal.* 2(9): 780–792. https://doi.org/10.1038/s41929-019-0317-4
14. Yu, F., Cangelosi, V. M., Zastrow, M. L., Tegoni, M., Plegaria, J. S., Tebo, A. G., Mocny, C. S., Ruckthong, L., Qayyum, H., Pecoraro, V. L., et al. (2014). Protein Design: Toward Functional Metalloenzymes. *Chem Rev.* 114(7): 3495–3578. https://doi.org/10.1021/cr400458x
15. Schwizer, F., Okamoto, Y., Heinisch, T., Gu, Y., Pellizzoni, M. M., Lebrun, V., Reuter, R., Köhler, V., Lewis, J. C., Ward, T. R., et al. (2017). Artificial Metalloenzymes: Reaction Scope and Optimization Strategies. *Chem Rev.* 118(1): 142–231. https://doi.org/10.1021/acs.chemrev.7b00014
16. Liang, A. D., Serrano-Plana, J., Peterson, R. L. and Ward, T. R. (2019). Artificial Metalloenzymes Based on the Biotin–Streptavidin Technology: Enzymatic Cascades and Directed Evolution. *Acc Chem Res.* 52(3): 585–595. https://doi.org/10.1021/acs.accounts.8b00618

17. Wu, T., Chen, X., Fei, Y., Huang, G., Deng, Y., Wang, Y., Yang, A., Chen, Z., Lemcoff, N. G., Feng, X., et al. (2025). Artificial metalloenzyme assembly in cellular compartments for enhanced catalysis. *Nat Chem Biol.* 21(5): 779–789. https://doi.org/10.1038/s41589-024-01819-7
18. Wu, T., Fei, Y., Deng, Y., Chen, X., Duan, Y., Liu, Y. and Bai, Y. (2025). Creation of Artificial Subcellular Organelles Using Compartmentalized *Escherichia coli* Bodies for Artificial Metalloenzyme-Mediated Abiotic Catalysis in Eukaryotic Cells. *J Am Chem Soc.* 147(18): 15229–15241. https://doi.org/10.1021/jacs.5c00473
19. Sivakumar, K., Xie, F., Cash, B. M., Long, S., Barnhill, H. N. and Wang, Q. (2004). A Fluorogenic 1,3-Dipolar Cycloaddition Reaction of 3-Azidocoumarins and Acetylenes. *Org Lett.* 6(24): 4603–4606. https://doi.org/10.1021/ol047955x
20. Kajetanowicz, A., Chatterjee, A., Reuter, R. and Ward, T. R. (2013). Biotinylated Metathesis Catalysts: Synthesis and Performance in Ring Closing Metathesis. *Catal Lett.* 144(3): 373–379. https://doi.org/10.1007/s10562-013-1179-z
21. Fischer, S., Ward, T. R. and Liang, A. D. (2021). Engineering a Metathesis-Catalyzing Artificial Metalloenzyme Based on HaloTag. *ACS Catal.* 11(10): 6343–6347. https://doi.org/10.1021/acscatal.1c01470
22. Mallin, H., Hestericová, M., Reuter, R. and Ward, T. R. (2016). Library design and screening protocol for artificial metalloenzymes based on the biotin-streptavidin technology. *Nat Protoc.* 11(5): 835–852. https://doi.org/10.1038/nprot.2016.019